Pergamon

Computers & Fluids Vol. 27, No. 1, pp. 11–28, 1998

Printed in Great Britain

PII: S0045-7930(97)00019-4

0045-7930/98 $19.00 + 0.00

A DETERMINISTIC FORCING SCHEME FOR DIRECT NUMERICAL SIMULATIONS OF TURBULENCE

M. R. OVERHOLT† and S. B. POPE

Sibley School of Mechanical and Aerospace Engineering, Cornell University, Ithaca, NY14853, U.S.A.

(Received 13 January 1997; in revised form 8 May 1997)

Abstract—Direct numerical simulations of statistically-stationary homogeneous isotropic turbulence require an artificial input of energy via a forcing scheme. Previous forcing methods based on a stochastic addition of energy have resulted in a poor representation of the energy-containing range of the energy spectrum function and significant temporal fluctuations of energy and other large-scale quantities. In this work a deterministic forcing scheme for direct numerical simulation is developed which uses wave number-dependent linear amplification of the lower-wave number modes, relaxing them over time toward a model energy spectrum function, which accurately represents grid turbulence. The scheme is shown to be robust and computationally efficient, resulting in velocity and scalar fields which quickly reach stationarity. It also has the significant advantages over stochastic forcing methods of not introducing additional statistical variability into the computations and allowing more physically realistic large-scale motions. © 1998 Elsevier Science Ltd. All rights reserved

1. INTRODUCTION

Direct numerical simulation (DNS) solves the exact flow equations without modeling and has been very useful in the study of mixing and reaction of scalars in homogeneous isotropic turbulence. Since the turbulent fields are random, in determining statistics it is advantageous to time-average to reduce statistical variability, which requires statistical stationarity of the flow. However, homogeneous isotropic turbulence is not stationary, so energy must be added to the largest scales via a forcing method, with the expectation that the small-scale quantities, which are of most interest, will not depend on the details of the large-scale dynamics, but only on its gross effects (e.g. the energy-addition rate).

All forcing methods rely on the cascade notion of Kolmogorov [1] for high Reynolds numbers, which states that the small scales of turbulence are independent of the details of the large-scale motions, solely depending on viscosity and on the rate of energy transfer from the large to the small scales. The high Reynolds number requirement is not met by most DNS, however, and so it is necessary to show that forcing can be justifiably used. Therefore, it is useful to compare the results of various forcing schemes, as is done in this study, to show that the details of the large-scale forcing has little if any effect on the small-scale statistics.

A number of forcing schemes have been previously developed for DNS and all take advantage of the pseudo-spectral nature of the computations. Siggia and Patterson [2] simply froze the magnitude (not the phase) of the lower-wave number modes at the desired value. Similarly, She *et al.* [3] introduced a scheme to maintain the total energy in each of the first two wave number shells ($1 \leq \kappa < 2$ and $2 \leq \kappa < 3$) constant in time, with the ratio between them consistent with the $\kappa^{-5/3}$ law. Chen *et al.* [4] report achieving stationarity of the velocity field in 5–10 eddy-turnover times using this scheme, which is a longer time than ideal. Note that both of these forcing schemes produce a variable energy addition rate, ϵ_i. A disadvantage of these schemes is that they also freeze the anisotropy in the large scales, making it difficult to achieve the isotropic statistics desired.

In 1981 Kerr [5] developed a simple deterministic scheme which forced the lower-wave number modes with a constant amplitude forcing coefficient, **f**, independent of the wave number. He forced all the Fourier modes with wave number components equal to zero or one. This scheme as well results in fluctuations in the energy addition rate, $\epsilon_i = \langle \mathbf{f} \cdot \mathbf{u} \rangle$ (where **u** is the velocity vector and the angled brackets denote the volume average). As pointed out by Vincent and Meneguzzi

†Author to whom all correspondence should be addressed.

[6] who used this scheme, owing to the ϵ_i fluctuations and discretization effects, one can only hope to reach statistical stationarity.

A more physically realistic forcing scheme is that developed by Siggia [7], who forced by a coupling to modes external to the DNS code that modeled the straining effects of large scales on smaller ones. However, this method yielded large fluctuations in the large-scale quantities which were correlated over long periods of time. More recently, Holzer and Siggia [8] and Pumir [9] introduced other physically-motivated forcing schemes.

The velocity field can also be forced stochastically. Eswaran and Pope [10] developed such a scheme (described in more detail in Section 2) and it has been used fairly extensively [11–15]. It has the advantages of yielding velocity fields with no gross anisotropy nor unreasonably high correlation times. However, forcing stochastically adds additional randomness into the flow with the associated disadvantages of preventing studies of the intrinsic chaotic nature of the flow and changing the variability of the random (turbulent) quantities.

Another stochastic forcing scheme, designed to lengthen the inertial subrange, was tested by Yakhot *et al.* [16]. Based on predictions from renormalization group theory, they use a white noise force with a power-law spectrum of κ^{-3}. However, although current stochastic forcing methods successfully achieve stationarity of the velocity field and in some ways are an improvement over former deterministic schemes, they significantly distort the large-scale motions resulting in a spectrum that does not well represent experimental data in the lower-wave number range. Forcing DNS in such a way incurs a number of disadvantages, not least of which is that the resulting statistics from large-scale quantities (such as the Reynolds stresses and scalar variance) do not correspond to natural turbulence. An obvious improvement would be to input the energy into the large scales such that the resulting spectrum is correct and if possible, to do it without incurring the disadvantages of the previous forcing schemes.

Suppose that there is a 'target' spectrum that the DNS is to conform to. This spectrum could be either from a decaying DNS run, from an experiment, or a model spectrum such as is introduced in this paper. Given such a spectrum, the deterministic forcing ideas of Kerr [5] and Siggia and Patterson [2] can be taken one step further, which is to force toward the specified target spectrum using a time-dependent, wave number-dependent forcing coefficient. Such a scheme would be dynamic, thereby allowing quick relaxation to stationarity and statistical isotropy; it would not introduce additional randomness into the flow; additionally, it would be general and straightforward to use in many different situations. These are the objectives of the forcing scheme formulated in this paper.

The paper is organized as follows. Section 2 develops and describes the deterministic forcing scheme and the model spectrum used and is followed by Sections 3 and 4 giving results and conclusions. Comparisons are made with the stochastically forced results of Overholt and Pope [15], who use the forcing scheme of Yeung and Pope [11].

2. NUMERICAL METHOD AND FORCING SCHEME

The DNS algorithm used is a fully parallelized version of the pseudo-spectral method of Rogallo [17] and is fully described in Overholt and Pope [15].

The full Navier–Stokes and scalar equations are solved without modeling on a three-dimensional grid, which is a cube of N^3 points with sides of length 2π in physical space. The pseudo-spectral method advances the solution in time in wave number space; however, the nonlinear products in the convection terms are formed in physical space, requiring discrete FFTs to transform the fields back and forth.

In order to resolve the smallest scales of the turbulent flow, it is required that $\kappa_{\max}\eta \geq 1.0$, where $\kappa_{\max}$ is the largest significant wave number, equal to $\sqrt{2}N\kappa_0/3$, κ_0 is the smallest wave number and η is the Kolmogorov length scale, the smallest length scale of the flow [18].

2.1. Stochastic forcing

The former forcing scheme for this DNS code stochastically forced the velocity field by adding acceleration increments to the largest scales only, such that continuity is satisfied and on average dissipation equals the artificial production. This results in the Reynolds number remaining

relatively constant throughout the simulation. Only the wave numbers inside a sphere of radius K_F are forced (excluding the origin). This forcing scheme introduces a forcing Reynolds number, R_F and a nondimensional time scale, T_F^*, into the simulation that can be varied to give a flow of the desired Reynolds number and large scale size (integral length scale l). This is the same forcing scheme as that used by Yeung and Pope [11], a refinement of that developed and tested by Eswaran and Pope [10]. In these works it is shown that the resulting velocity fields are stationary and isotropic, to a good approximation. In this paper the results of the above stochastic forcing scheme are compared with those obtained using the new deterministic scheme to be formulated.

2.2. *A model energy spectrum*

A model energy spectrum can be constructed as follows [19]:

$$E_m(\kappa) = C\epsilon^{2/3}\kappa^{-5/3} f_L(\kappa L) f_\eta(\kappa\eta), \tag{1}$$

where f_L and f_η are specified nondimensional functions. The function f_L determines the shape of the energy-containing range and tends to unity for large κL. The integral scale, L, used here is defined as $k^{3/2}/\epsilon$. Similarly, f_η determines the shape of the dissipation range and it tends to unity for small $\kappa\eta$. In the inertial subrange both f_L and f_η are essentially unity and so the Kolmogorov $-5/3$ spectrum with constant C is recovered.

The specification of f_L is:

$$f_L(\kappa L) = \left\{ \frac{\kappa L}{[(\kappa L)^2 + c_L]^{1/2}} \right\}^{5/3+p_0}, \tag{2}$$

where p_0 is taken to be 4 and c_L is a positive constant. Clearly f_L tends to unity for large κL, while the exponent $5/3 + p_0$ leads to $E_m(\kappa)$ varying as $\kappa^{p_0} = \kappa^4$ for small κL. (The alternative choice $p_0 = 2$ leads to $E_m(\kappa) \sim \kappa^2$ for small κ).

The specification of f_η is:

$$f_\eta(\kappa\eta) = \exp\{-\beta([(\kappa\eta)^4 + c_\eta^4]^{1/4} - c_\eta)\}, \tag{3}$$

where β and c_η are positive constants. Note that for $c_\eta = 0$, this reduces to:

$$f_\eta(\kappa\eta) = \exp(-\beta\kappa\eta). \tag{4}$$

Because the velocity field is infinitely differentiable, it follows that for large κ, the spectrum decays more rapidly than any power of κ; hence, the exponential decay. Several experiments support the exponential form with $\beta = 5.2$ [20]. However, the simple exponent [Equation (4)] departs from unity too rapidly for small $\kappa\eta$, a defect that is remedied by Equation (3).

For specified values of k, ϵ and ν, the model spectrum is determined by Equations (1)–(3) with $C = 1.5$ and $\beta = 5.2$. The constants c_L and c_η are determined such that $E_m(\kappa)$ and $2\nu k^2 E_m(\kappa)$ integrate to k and ϵ, respectively. Alternatively, the nondimensional model spectrum is uniquely determined by a specified value of the Taylor-scale Reynolds number, Re_λ, or by the separation between the integral and Kolmogorov scales. This last specification is the most natural for DNS since it allows direct specification of both the small-scale resolution and the number of integral scales in the computational domain.

In Fig. 1, the model spectrum is compared with the experimental data of Comte-Bellot and Corrsin [21]. A fourth-order departure from zero of the model spectrum is used ($p_0 = 4$). Overall, the agreement is very good, although there are slight differences in slope in the transitional region between the large and small scales. The experimental data seems to have a marked change in curvature in this region (at wave number $\kappa\eta \approx 0.2$), which is smoothed out by the model spectrum. This small difference is of little importance for DNS, assuming that the higher-wave number range is not forced.

2.3. *The forcing scheme*

The purpose of the forcing scheme is to add energy to the lower-wave number modes such that each of these modes evolves over time in a smooth way until it reaches its target value, as

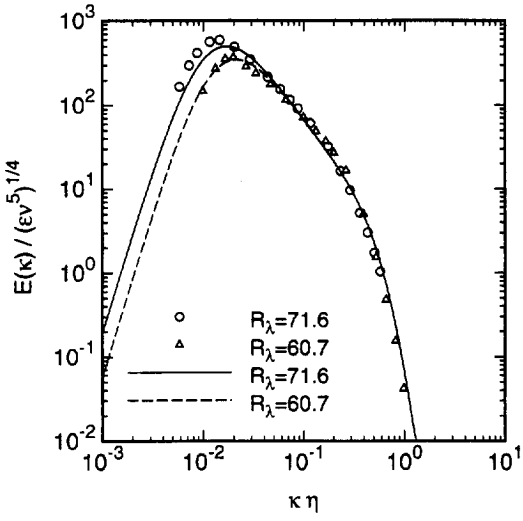

Fig. 1. Energy spectrum function model (lines) and experimental data of Comte–Bellot and Corrsin (symbols) [21], with Kolmogorov scaling.

given by the model spectrum just defined. If perturbed from the model value, it should return quickly with a minimum of fluctuation.

We accomplish energy addition by linear amplification of the velocity field in wave number space using a nondimensional *forcing coefficient*, f_κ. This coefficient is a scalar quantity, which results in the phase of the amplified velocity remaining unchanged. Smooth evolution of the spectrum modes is accomplished by governing the forcing coefficient evolution by a differential equation. In such a system, if the amplification of the velocity magnitudes remains small and the resulting spectrum has the right shape, then the large-scale motions should be physically realistic to a first approximation at least.

2.3.1. Forcing coefficient, f_κ. The velocities in wave number space evolve via the differential equation:

$$\frac{\partial \hat{\mathbf{u}}(\kappa_1, \kappa_2, \kappa_3, t)}{\partial t} = \hat{\mathbf{a}}(\kappa_1, \kappa_2, \kappa_3, t) + \frac{f_\kappa(t)}{\tau}\hat{\mathbf{u}}(\kappa_1, \kappa_2, \kappa_3, t), \tag{5}$$

where $\hat{\mathbf{a}}$ is the contribution from the Navier–Stokes equation and τ is the forcing time scale. Since we are forcing the spectrum, the forcing coefficient is parameterized by κ, which is the magnitude of the wave number vector $\boldsymbol{\kappa}$. Therefore, each wave number magnitude κ has its own forcing coefficient, f_κ, which evolves independently according to its own evolution equation. For DNS with a domain length of 2π, κ is discretized into integer magnitudes (e.g. a 32^3 simulation will have forcing coefficients f_1–f_{16}).

A simple ordinary differential equation for the evolution of each forcing coefficient is chosen so that the dynamics (similar to a mass-spring-damper) can be easily understood and so that the number of parameters defining the scheme is kept to a minimum. The equation for $f_\kappa(t)$ is:

$$\frac{\mathrm{d}f_\kappa(t)}{\mathrm{d}t} = P\left[\frac{-1}{\tau}\ln\left(\frac{E(\kappa;t)}{E_m(\kappa)Z_f(\kappa)}\right) - \alpha\alpha_c f_\kappa(t)\right], \tag{6}$$

$$= P[S_\kappa], \tag{7}$$

where $E(\kappa;t)$ is the spectrum from the DNS, Z_f is a forcing cut-off function to be defined, α is a nondimensional damping coefficient and α_c is the critical damping coefficient. The operator P is defined as follows:

$$P(S_\kappa) = \begin{cases} S_\kappa, \text{ for } f_\kappa > 0 \\ S_\kappa, \text{ for } f_\kappa = 0 \text{ and } S_\kappa > 0 \\ 0, \text{ for } f_\kappa = 0 \text{ and } S_\kappa \leq 0. \end{cases} \tag{8}$$

Thus, f_κ can never become negative. This achieves two purposes. For one, it ensures that energy is only added and not removed; secondly, it allows Z_f to go to zero for $\kappa \geq \kappa_f$, thus accomplishing the forcing cut-off as will be seen.

With the Heaviside function defined by:

$$H(x) = \begin{cases} 1, \text{ for } x > 0 \\ 0, \text{ for } x \leq 0, \end{cases} \tag{9}$$

we have

$$\frac{df_\kappa(t)}{dt} = \{H(f_\kappa) + [1 - H(f_\kappa)]H(S_\kappa)\}S_\kappa. \tag{10}$$

To define the model spectrum, $E_m(\kappa)$, the separation between the integral and Kolmogorov scales is needed. This is achieved by two forcing parameters which must be specified, κ_η^* and E_L^*. DNS small-scale resolution is measured by $\kappa_{max}\eta$, which is analogous to κ_η^*. Since the grid size, N, determines κ_{max}, the specification of κ_η^* yields η. The integral-scale size, then, is given by E_L^*, which is defined as the fraction of the total energy captured by the simulation. Equivalently, we can find κ_0, the smallest wave number:

$$\int_{\kappa_0}^{\infty} E_m(\kappa)\, d\kappa = E_L^* \int_0^{\infty} E_m(\kappa)\, d\kappa. \tag{11}$$

2.3.2. Wave numbers forced. Forcing is limited to the range of wave numbers $(0, \kappa_f)$ via the forcing cut-off function, Z_f, which is defined as:

$$Z_f(\kappa; \kappa_f, \zeta) = \tanh\left(\frac{\kappa_f - \kappa}{\zeta\kappa_f}\right) H(\kappa_f - \kappa), \tag{12}$$

where ζ is a parameter that determines the abruptness of the cut-off. Figure 2 shows this function for several values of ζ. The use of a forcing cut-off function has the additional advantage that the model spectrum is not required to have the correct shape in the dissipation range (or for $\kappa \geq \kappa_f$).

The cut-off wave number is implicitly defined via a third forcing parameter which must be specified, E_f^*, the fraction of energy to be forced:

$$\int_0^{\kappa_f} E_m(\kappa)\, d\kappa = E_f^* \int_0^{\infty} E_m(\kappa)\, d\kappa. \tag{13}$$

Additionally, the width of the cut-off function, ζ, is needed. A minimum value for ζ, found experimentally, is about 0.2. Smaller values make the forcing cut-off too abrupt, potentially resulting in a kink in the DNS spectrum, $E(\kappa;t)$.

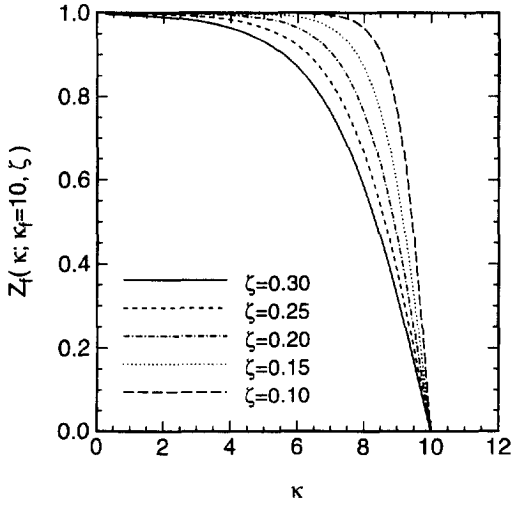

Fig. 2. Forcing cut-off function Z_f for $\kappa_f = 10$, showing the effect of varying the width parameter, ζ.

2.3.3. Damping coefficient, α. Damping is necessary in order to achieve statistical stationarity as soon as possible and to minimize the amount of oscillation of the system. Some damping is already present since by the cascade notion of turbulence energy is transferred from the large to the small scales and hence from one wave number mode and its f_κ to another. However, to achieve critical damping, which will give the minimum time to stationarity for a given τ, damping must be added to the system and this is done through the forcing parameters α and α_c.

From a linear stability analysis (see Appendix A), a relationship for critical damping, α_c, can be found as $\alpha_c = 2\sqrt{2}/\tau$. The analysis assumes independence of the differential equations governing each f_κ and models the effect of the Navier–Stokes equations as simply an energy sink.

With α_c determined, α can be specified between zero and one to give zero (added damping) to critical damping. In Section 3, we will experimentally determine α for critical damping and see that it is close to one and grid independent, thereby verifying this analytical result. An additional effect of damping is to change the stationary solution or fixed point of the system. This is evident from Equation (6) with the left side set to zero (see Appendix A for details). As damping or the time scale increases, the stationary solution for $E(\kappa;t)$ falls below $E_m(\kappa)$, though slowly.

2.3.4. Forcing time scale, τ. The parameter τ is the only one that directly depends on the Reynolds number. It is expected to be a function of the time scale of the turbulence, which is Reynolds-number dependent. The question is, which time scale of the turbulence does it depend on?

The most logical time scale may appear to be k/ϵ since that is the time scale of the energy-containing range where action against the mean gradients produces turbulent kinetic energy in a turbulent shear flow. However, that is not the correct time scale to use here since the energy input into the flow is via another mechanism. The purpose of τ in our forcing scheme is to govern the response of the forcing coefficients to the changes over time in the turbulent flow (and hence in the energy spectrum). Without any forcing the turbulent kinetic energy would simply decay due to dissipation, which occurs in the high-wave number range. Therefore, the forcing must respond to the dissipation dynamics, which is why the Kolmogorov time scale, τ_η, is the appropriate one to normalize by. Hence, the time scale coefficient, T_f^*, is defined as:

$$T_f^* = \left(\frac{\tau}{\tau_\eta}\right). \tag{14}$$

From another perspective, it is important for the stability of the system that the time scale of the forcing be smaller than the smallest time scale of the flow, which is τ_η. The results clearly bear out that this is the correct normalization.

2.3.5. Implementation details. In implementing this forcing scheme, it should be noted that the spectrum, $E(\kappa;t)$, does not need to be calculated at every step to get good forcing scheme accuracy. The evolution of the forcing coefficients and the velocity field statistics when $E(\kappa;t)$ is calculated at every step and when it is only calculated every two or three steps is indistinguishable. Specifically, we calculate $E(\kappa;t)$ once every M_T steps. Since the dominant computational cost for this forcing scheme is in calculating $E(\kappa;t)$, a value of three for M_T results in nearly a two-thirds reduction in computational cost.

The time step for velocity advancement in the DNS code is determined by the CFL condition. This condition also governs the change in the spectrum, $E(\kappa;t)$. Therefore, for a given CFL number the value of M_T required for a certain accuracy will not change with the grid size. So, for a given M_T, this forcing scheme becomes more costly as grid size increases. However, proportionally the cost remains a very small constant since it scales with the time-advancement costs of DNS.

A complete list of parameters for this scheme, then, is as follows:

1. κ_η^*, small-scale resolution parameter;
2. E_L^*, fraction of energy captured;
3. E_f^*, fraction of energy forced;
4. T_f^*, normalized forcing time scale;
5. α, normalized damping coefficient;
6. ζ, width of the cut-off function.

Table 1. Forcing parameter test results

Run	N	κ_η^*	E_L^*	E_f^*	T_f^*	α	κ_f	$\kappa_{max}\eta$	l	Re_λ	k
ℓ1	32	0.68	0.95	0.67	0.30	0.70	5.16	1.10	1.07	22.2	1.01
ℓ2	32	0.70	0.85	0.67	0.30	0.70	3.66	1.10	1.49	33.5	1.51
ℓ3	32	0.72	0.75	0.67	0.30	0.70	2.82	1.10	1.72	41.3	1.84
ℓ4	64	0.72	0.85	0.67	0.30	0.70	4.25	1.09	1.33	65.4	12.1
ℓ5	64	0.74	0.75	0.67	0.30	0.70	3.64	1.02	1.59	76.9	15.8
f1	32	0.78	0.95	0.80	0.30	0.70	6.44	1.12	1.13	19.6	0.84
f2	32	0.88	0.95	0.90	0.30	0.70	7.96	1.12	1.04	16.8	0.73
f3	64	0.78	0.95	0.80	0.30	0.70	8.84	1.13	1.11	40.6	6.97
f4	64	1.04	0.95	0.99	0.30	0.70	20.6	1.12	0.93	27.3	4.74
T1	32	0.68	0.95	0.67	0.10	0.35	5.16	1.08	1.03	22.7	1.06
T2	64	0.68	0.95	0.67	0.10	0.35	5.71	1.11	1.04	47.1	8.45
T3	128	0.68	0.95	0.67	0.10	0.35	7.37	1.00	0.91	86.2	75.0
T4	32	0.68	0.95	0.67	0.50	0.35	5.16	1.10	1.01	22.2	1.02
T5	64	0.68	0.95	0.67	0.50	0.35	5.71	1.08	1.04	46.4	8.77
T6	128	0.68	0.95	0.67	0.50	0.35	7.37	1.01	0.91	85.6	73.8
T7	32	0.68	0.95	0.67	0.30	0.35	5.16	1.09	1.02	22.4	1.04
T8	32	0.68	0.95	0.67	0.70	0.35	5.16	1.10	1.02	22.0	1.00
a1	32	0.68	0.95	0.67	0.70	0.20	5.16	1.17	1.14	22.7	0.90
a2	32	0.68	0.95	0.67	0.70	0.35	5.16	1.18	1.15	22.4	0.88
a3	32	0.68	0.95	0.67	0.70	0.50	5.16	1.18	1.15	22.2	0.86
a4	32	0.68	0.95	0.67	0.70	0.65	5.16	1.19	1.15	21.9	0.84
a5	32	0.68	0.95	0.67	0.70	0.80	5.16	1.20	1.15	21.6	0.81
a6	64	0.68	0.95	0.67	0.70	0.35	5.71	1.21	1.14	47.0	7.01

3. RESULTS

This section consists of the results of a number of numerical tests run on grid sizes of 32^3 to 128^3, followed by three longer simulations for comparison with the stochastically forced results of Overholt and Pope [15].

All the simulations appearing in Table 1 that have N less than 128 start from a randomly specified initial velocity field. This field is generated subject to the constraints of continuity and isotropy, according to a prescribed energy spectrum function (not the model spectrum of this paper) [17]. In the case of the 128^3 tests, the initial velocity field came from a previous simulation in order to shorten the time to stationarity.

For the longer comparative simulations represented in Tables 2–4, the initial velocity and scalar fields are first allowed to evolve for a number of eddy-turnover times until statistically stationary. The runs are then begun and the data is averaged over time as well as space to generate the results shown.

Table 2. Run parameters and statistics. Angle brackets ⟨⟩ denote the time-averaged stationary value

Parameter	Tabulated	Run 32D.3	Run64DL	Run 64DLL
N, grid size	N	32	64	64
n, number of simulations	n	16	4	4
ν, kinematic viscosity	ν	0.025	0.025	0.025
Pr, Prandtl number	Pr	0.7	0.7	0.7
β, mean scalar gradient ($d\langle\phi\rangle/dy$)	β	1.0	1.0	1.0
κ_f, largest forced wave number	κ_f/κ_0	4.78	8.41	11.2
κ_{max}, largest resolved wave number	$\kappa_{max}\langle\eta\rangle$	1.03	1.47	1.08
κ_0, smallest wave number	$\kappa_0\langle\eta\rangle$	0.0682	0.0486	0.0358
$l \equiv (1/3)L_{i,i}$, integral length scale	$\kappa_0\langle l\rangle$	1.20	0.888	0.685
$L_\epsilon \equiv u'^3/\epsilon$, turbulent length scale	$\langle L_\epsilon/l\rangle$	1.01	0.956	0.964
λ, Taylor microscale	$\langle\lambda/l\rangle$	0.578	0.550	0.536
η, Kolmogorov length scale	$\langle\eta/l\rangle$	0.0568	0.0547	0.0522
T_E, eddy turnover time	$\langle l/u'\rangle$	1.25	0.671	0.371
τ_η, Kolmogorov time scale	$\langle\tau_\eta\rangle/T_E$	0.148	0.141	0.138
T, duration of the stationary period	T/T_E	26.6	19.4	32.8
k, turbulent kinetic energy	$\langle k\rangle$	1.37	2.67	5.11
$u' \equiv (2k/3)^{1/2}$, turbulence intensity	u'	0.957	1.33	1.84
v', v-velocity rms value	$\langle v'\rangle$	0.954	1.34	1.85
ϵ, dissipation	$\langle\epsilon\rangle$	0.721	2.79	9.51
$Re_l \equiv u'l/\nu$, Reynolds number	$\langle Re_l\rangle$	46.2	47.5	50.6
$Re_\lambda \equiv u'\lambda/\nu$, Taylor Reynolds number	$\langle Re_\lambda\rangle$	26.6	26.1	27.1
$\langle v\phi\rangle$, scalar flux	$\langle v\phi\rangle$	−0.877	−0.955	−1.00
$\langle\phi^2\rangle$, scalar variance	$\langle\phi^2\rangle$	2.01	1.30	0.787
ϕ', scalar rms value	$\langle\phi^2\rangle^{1/2}$	1.42	1.14	0.887
rms $(\partial\phi/\partial y)$, scalar gradient rms	$\langle(\partial\phi/\partial y)^2\rangle^{1/2}$	2.90	3.07	3.15
ϵ_ϕ, scalar dissipation	$\langle\epsilon_\phi\rangle$	0.870	0.969	1.01
$r \equiv 2k/\epsilon/\langle\phi^2\rangle/\epsilon_\phi$, time scale ratio	$\langle r\rangle$	1.67	1.45	1.40

Table 3. Forcing parameters for the deterministically-forced runs

Parameter	Run 32D.3	Run 64DL	Run 64DLL
κ_n^*	0.64	1.00	0.72
E_L^*	0.935	0.97	0.99
E_f^*	0.67	0.80	0.80
T_f^*	0.40	0.40	0.40
α	0.25	0.70	0.70
ζ	0.25	0.25	0.25
M_T	1	2	2

The objectives of the numerical tests and longer simulations are:

1. to determine the dynamic behavior of the forcing system as a function of the forcing parameters;
2. to confirm the grid independence of the forcing parameters;
3. to compare the results with those obtained using stochastic forcing.

3.1. Dynamic behaviour and the forcing parameters

There are six forcing parameters and the implementation parameter M_T. Five of the forcing parameters will be examined here; the remaining parameters, ζ and M_T, have already been sufficiently addressed in Section 2. A number of runs were made for the numerical tests; their forcing parameters and a few velocity field statistics are summarized in Table 1. In each case the number of simulations, n, was 1, with a ζ of 0.25 and an M_T of 1.

3.1.1. Large-scale resolution and E_L^*. One of the motivations for this forcing scheme was the need to force the large scales more naturally. The parameter E_L^* gives direct control over how much of the low-wave number range of the spectrum is simulated. Therefore, if statistics of the large scales are important, E_L^* should be close to one. This topic is addressed directly in Section 3.2.

The integral-scale size is also directly affected by E_L^*. Runs $\ell 1$ to $\ell 5$ demonstrate this dependence. Since κ_0 is fixed at one by the pseudo-spectral method, increasing E_L^* pushes the peak of the spectrum to higher and higher wave numbers, thereby decreasing the integral scale and the Reynolds number (assuming, of course, that all of the other parameters are held constant). The effect of E_L^* on the integral scale is also independent of grid size since as seen in Table 1 the integral scales for runs $\ell 2$ and $\ell 4$ as well as for runs $\ell 3$ and $\ell 5$ are the same within statistical error (see also runs f1 and f3).

3.1.2. Largest forced wave number, κ_f. In contrast to E_L^*, the criteria for choosing E_f^* is not as clear. With earlier forcing methods a minimum number of wave number modes were forced (κ_f as small as possible) in order not to interfere with the small-scale statistics. However, with a forcing scheme that correctly reproduces the entire spectrum that argument is not as strong.

Runs $\ell 1$ and f1 to f4 with the accompanying Fig. 3 show the effect of varying κ_f. Since $\kappa_{max}\eta$ is 1.1 for each case the spectra are the same in the higher-wave number range. However, it is obvious that the DNS spectrum does not exactly match the model since the number of modes forced affects the spectrum shape. The difference between the DNS and the model spectra is that the DNS spectrum drops off to exponential decay at a lower-wave number than the model, with the result that κ_f determines where the knee in the spectrum will be. Therefore, it may again be wise to force only a small portion of the spectrum and allow the higher-wave number modes to evolve on their own.

Table 4. Forcing parameters for the stochastically-forced run of Overholt and Pope [15]

Parameter	Run 32.3
$R_F \equiv \epsilon^{*1/3}\kappa_0^{4/3}/\nu$	5.704
$T_F^* \equiv T_F \epsilon^{*1/3}\kappa_0^{2/3}$	0.1497
ϵ^*	0.0029
K_F	$2\sqrt{2}$

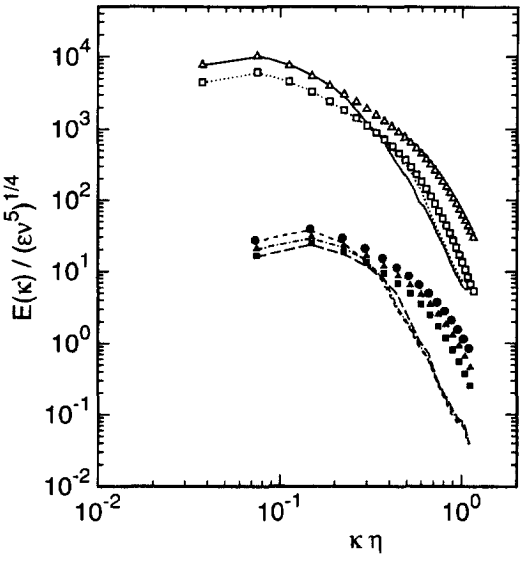

Fig. 3. Energy spectrum functions for runs $\ell 1$ and f1–f4, with Kolmogorov scaling, showing the effect of varying the fraction of energy forced, E_f^*. The curves for $N = 64$ have been shifted up two decades. E, lines; E_m, symbols. - - -, $E_f^* = 0.67$; – · –, $E_f^* = 0.80$; — — —, $E_f^* = 0.90$; ———, $E_f^* = 0.80$; ···, $E_f^* = 0.99$.

We also see that κ_η^* is a function of E_f^*. As E_f^* decreases, the height of the spectrum increases and hence κ_η^* must be decreased to keep the higher-wave number range at the same level, thereby keeping $\kappa_{max}\eta$ fixed.

The question of whether forcing more or less of the spectrum interferes with the results has yet to be addressed. No obvious effects were seen in the results for the tests done. For E_L^* values of 0.95 or less an E_f^* of 0.67 appears satisfactory and is used throughout.

3.1.3. Small-scale resolution and κ_η^*. As discussed earlier, $\kappa_{max}\eta \geq 1.0$ is required for spatial resolution of the smallest velocity scales in the turbulent flow field [18]. The parameter κ_η^* specifies just this value; however, since the final DNS spectrum is not the same as the model spectrum (unless all the wave numbers are forced) there is a scaling involved.

Throughout these tests, κ_η^* has been adjusted to give $\kappa_{max}\eta \approx 1.1$. As can be seen in Table 1, the difference between $\kappa_{max}\eta$ and κ_η^* increases as κ_f decreases (for a fixed grid size). This does not present a problem in actual use for two reasons, however. First of all, to a first approximation κ_η^* can be scaled by $1.1/E_f^*$ to remove its dependence on E_f^*. Secondly, one typically uses one value of E_f^* (and hence a single κ_η^*, easily found by trial and error) for a number of simulations and the coupling between κ_η^* and E_f^* has only a slight grid-dependence.

3.1.4. Time scale, T_f^*. The forcing time scale is key to the behavior of this forcing system. If it is much smaller than the smallest turbulence time scale ($T_f^* \ll 1$), then essentially the spectrum is reset to the model value at each time step, with large values and derivatives of the forcing coefficients if T_f^* is too small. If it is larger than the smallest time scale ($T_f^* > 1$), then the system will become unstable, oscillating with increasingly greater amplitude.

Our objectives here are to observe qualitatively how the system behaves as a function of T_f^* and to explore the range of usable values. To that end runs T1 to T8 demonstrate the behavior at various values of T_f^* and for various grid sizes (Figs 4–6). The evolution of mode $\kappa = 3$ is shown in each case and is representative of the behavior of all the forced modes. The damping coefficient for all the T-runs is set at half the critical value, as determined in the next subsection. This is done so that some oscillation is possible, to illuminate the effect of T_f^* on the dynamic behavior, while keeping the system well-behaved.

Figure 4 shows the results for all the 32^3 runs and for a wide range of T_f^* values. As expected, as the time scale increases, the system oscillates with greater amplitude, heading towards instability. In fact, without damping run T8 ($T_f^* = 0.70$) would oscillate very badly.

From these runs, we can also establish the Re-independence of the time scale normalization. The first three runs, T1 to T3, are for a small time scale of 0.10 and clearly show the forced

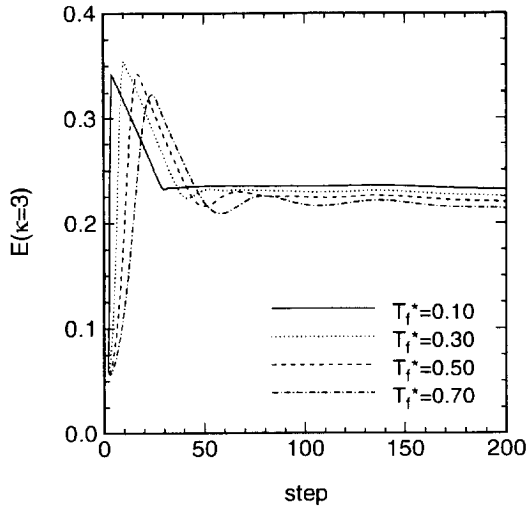

Fig. 4. Evolution of the spectrum mode $\kappa = 3$ for runs T1, T4, T7 and T8, showing the effect of varying the forcing time scale, T_f^*. The other forced modes behave similarly.

spectrum modes very swiftly reaching stationarity at the model values for each grid size (see Figs 4–6). The behavior upon reaching the model value is identical in each case, with just the slightest oscillation and then stationarity.

Note that the modes for the two larger grid sizes continue to evolve slowly upward after the initial behavior just described, strictly speaking not reaching stationarity until the end of the run. This is due to the initial condition being far from the final state and hence having a Kolmogorov length scale that is too large. This length scale normalizes the model spectrum. Therefore, a slow feedback mechanism is seen in which the model spectrum evolution and the Kolmogorov length scale evolution are synchronous. This situation can be easily avoided by choosing an initial condition closer to the final state.

The next three runs, T4 to T6, are for a larger time scale of 0.50. Here the responses of the forcing coefficients are slower and hence it takes longer to reach stationarity. In each figure, the decay rates of the curves are the same once they overshoot the model value and reach a maximum, but the time required to reach that maximum value is directly proportional to T_f^*.

It is evident in each case that the dynamic response of the system at the various Reynolds numbers is identical for a given T_f^* and hence we can conclude that τ_f does indeed scale with τ_η, making T_f^* Re-independent.

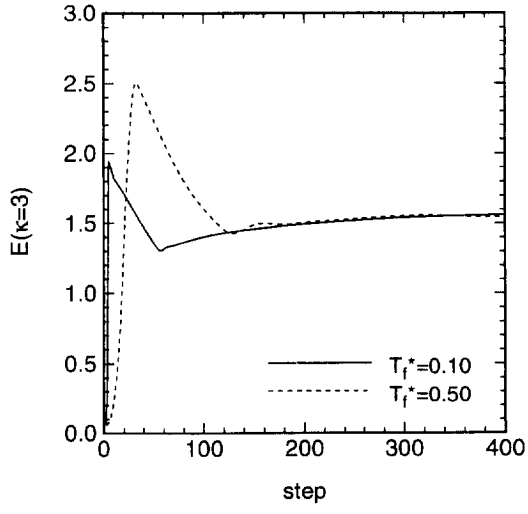

Fig. 5. Evolution of the spectrum mode $\kappa = 3$ for runs T2 and T5. Compare the initial response with the results in Figs 4 and 6.

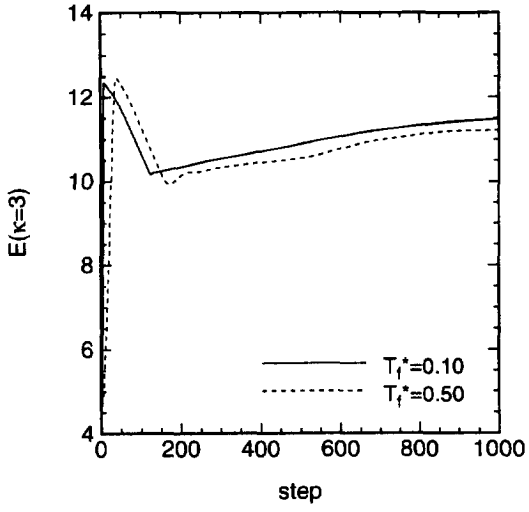

Fig. 6. Evolution of the spectrum mode $\kappa = 3$ for runs T3 and T6. Compare the initial response with the results in Figs 4 and 5.

The purpose of having a forcing time scale is to allow one to tailor the dynamic behavior of the system to meet one's needs. However, without damping, T_f^* must be chosen instead to provide stability to the system. This leads directly to a look at the damping coefficient. As has been seen, given proper damping it is possible to use a wide range of values of T_f^* between zero and one.

3.1.5. Damping coefficient, α. Earlier we derived the critical damping coefficient, α_c, using a linear stability analysis on a simplified forcing system. However, it should also be possible to estimate this value directly from the evolution of the spectrum modes. We attempt to do that here.

We begin by modifying the forcing algorithm slightly to allow all values of f_κ, both energy addition and energy removal, thereby enabling normal oscillation of the spectrum modes [i.e. $P(S_\kappa) \equiv S_\kappa$ in Equation (8)]. Using the largest value of T_f^* examined in the previous runs, 0.70, runs a1 to a5 show the evolution of mode $\kappa = 3$ for increasing values of α.

Critical damping is defined as the smallest value of α that does not result in overshoot. In Fig. 7, damping obviously strongly affects the mode evolution and the system appears to cross the critical damping value somewhere between 0.65 and 0.80. Therefore, a value of 0.70 was taken to be close to the critical value and used as such for the other test runs.

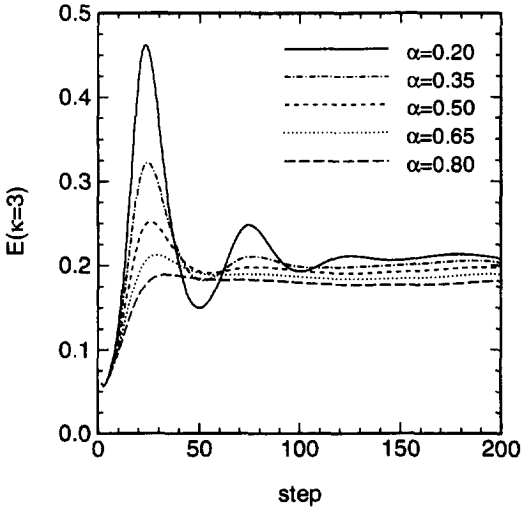

Fig. 7. Evolution of the spectrum mode $\kappa = 3$ for runs a1–a5, showing the effect of varying the damping coefficient, α, with both energy addition and removal [i.e. $P(S_\kappa) \equiv S_\kappa$ in Equation (8)]. The other forced modes behave similarly.

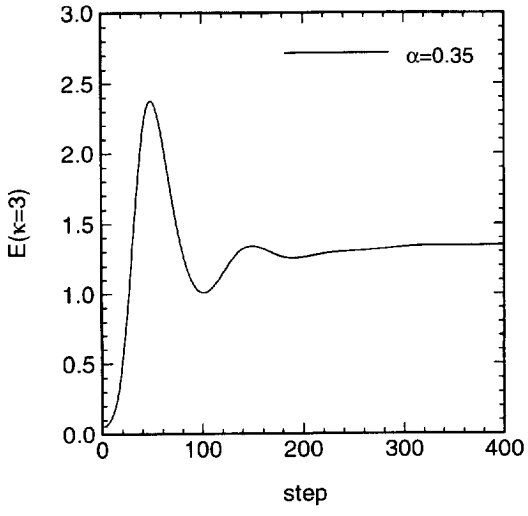

Fig. 8. Evolution of the spectrum mode $\kappa = 3$ for run a6, with both energy addition and removal. Compare the initial response with the results Fig. 7.

These results are for a specific grid size, of course, but run a6 for a 64^3 grid in Fig. 8 shows an identical dynamic behavior as run a2 in Fig. 7, giving strong evidence that Equation (A.9) (see Appendix A) is a grid-independent scaling. It is also noticeable in Figs 4 and 7 that the stationary state is a function of both the damping and the time scale, with the stronger-damped and larger time scale cases having a slightly lower stationary value. This is as predicted by the linear analysis and Equation (A.11).

For grid sizes of 64^3 and smaller, the time to stationarity from the standard initial condition to the model spectrum (for reasonable parameter choices) is small and not a concern. However, for larger grids and their associated Reynolds numbers the standard initial condition becomes farther and farther from the desired stationary spectrum, thereby introducing two potential problems. First, the large differences will cause very large transient forcing coefficient values and much oscillation, depending on the damping. Second, the large changes needed will simply take time to occur, thereby incurring large CPU costs before reaching stationarity. Such an approach is not necessary. Obviously a better initial condition is needed. One option is to use the model

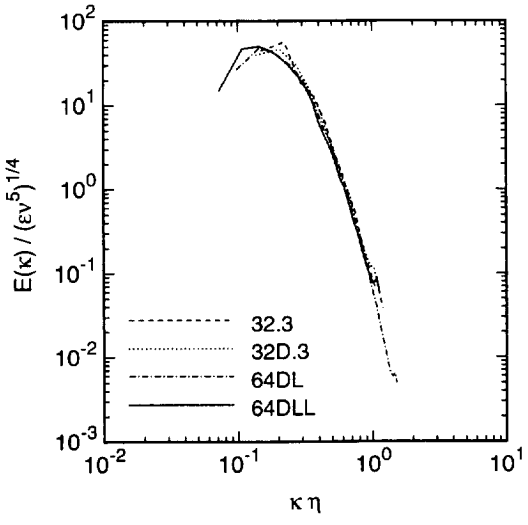

Fig. 9. Spectra from runs 32.3, 32D.3, 64DL and 64DLL, with Kolmogorov scaling. Data for run 32.3 is from Overholt and Pope [15]. Run 32D.3 mimics run 32.3, while runs 64DL and 64DLL capture more energy. Note that run 64DL is over-resolved.

spectrum to randomly set an initial condition, in a similar way as for the initial condition used in this paper. That would allow the fastest convergence.

A previous velocity field can also be used as the initial condition as was done for the 128^3 runs here. In that case to minimize the time to stationarity a small value of T_f^* should be used along with critical damping until the spectrum reaches stationarity, after which T_f^* (and α) can be set to the value(s) desired.

3.2. Comparison with stochastic results

Now that the dynamic behavior of this forcing system is well understood, what do the results look like? To answer this question we compare results from three longer full simulations to the stochastically forced run of Overholt and Pope [15] named 32.3, a work which investigates the mixing of a passive scalar with a mean scalar gradient, β. In each case, the Reynolds numbers of the two systems were matched as closely as possible and in the case of run 32D.3, E_L^* and E_f^* were chosen to approximately match the spectra of the two runs as well. Table 2 provides a summary of the simulations performed and of the definitions and values of the primary quantities characterizing the flow. The forcing parameter values are given in Tables 3 and 4.

One of the primary motivations for developing this new forcing method was the need for less statistical variability in the simulations. Confidence intervals give a direct measure of this property and were compared for a number of velocity and scalar statistics from the 32.3 and 32D.3 runs. Of 39 velocity field statistics examined, 85% had smaller confidence intervals; similarly, 69% of 29 scalar field statistics had less statistical variability. From these results alone, we can conclude that this forcing method successfully reduces the statistical variability since these two simulations give essentially the same averaged results.

Nearly all of the quantities appearing in the previous work by Overholt and Pope [15] were calculated for run 32D.3 and compared. Without exception the two results were qualitatively identical and quantitatively extremely close, with all of the new results having either similar variability or less. A few example figures follow.

Figure 9 shows the spectra from these four runs. The main difference between them is how much of the low-wave number range of the complete spectrum is captured or represented (with run 64DL over-resolving the small scales). A concern of any forcing method for isotropic DNS studies is the resultant isotropy of the velocity fields. It is clear from the formulation that this forcing method is isotropic. However, that alone does not guarantee isotropy; the numerical implementation must also be consistent. We have succeeded in gaining isotropic fields, at least to the extent possible in DNS with a rectangular domain [10] and this is evident in the one-dimensional spectra shown in Fig. 10.

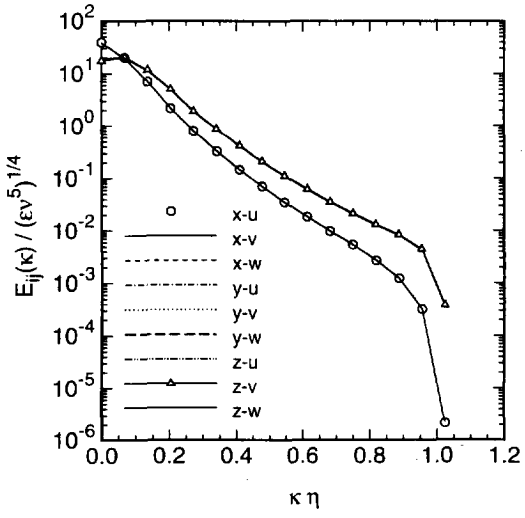

Fig. 10. One-dimensional spectra for velocity, consistent with isotropy. The legend gives the direction and velocity component of each curve.

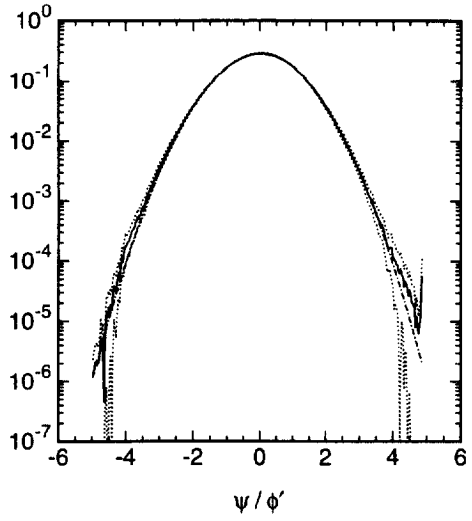

Fig. 11. Scalar pdf for run 32D.3. ···, 90% confidence intervals; – · –, Gaussian.

One of the difficulties of studying pdf tails is the rarity of the large fluctuations which compose them and hence their high statistical variability. The scalar pdf tails in the previous paper were plagued with bumps and such because of this; however, the scalar pdf in Fig. 11 has much smaller confidence intervals and smoother tails, which is characteristic of the other pdf tails examined.

Some of the conditional quantities showed less fluctuation at their extremes for the new forcing method. An example is the conditional expectation of the laplacian of the scalar, given both the scalar and v-velocity values, shown in Fig. 12. The linear model proposed by Overholt and Pope [15] for this quantity is:

$$\frac{\nabla^2\phi}{\langle\epsilon_\phi\rangle/(\Gamma\phi')} = a\frac{\phi}{\phi'} + b\frac{v}{v'} + \xi, \tag{15}$$

where ϕ' is the scalar rms value, v' is the v-velocity root mean square value and ξ is a zero-mean random variable uncorrelated with v and ϕ. Contours from this model overlay the data in Fig. 12 and show a fit identical to that seen in Overholt and Pope [15].

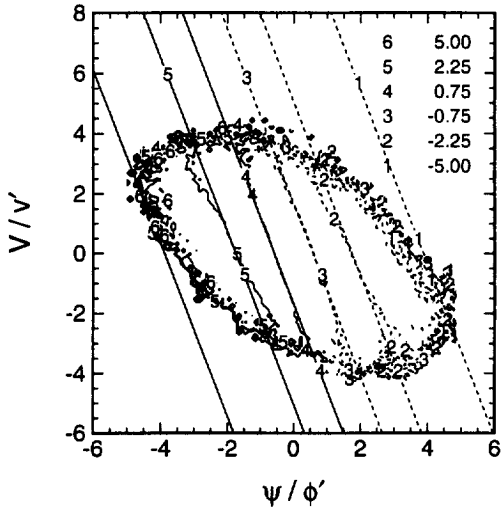

Fig. 12. Expectation of the normalized $\nabla^2\phi$ jointly conditioned on ϕ and v-velocity, overlaid with contours from the linear model of Overholt and Pope [15], with coefficients $a = -1.288$ and $b = -0.446$. The accessed region is inside the oval shape.

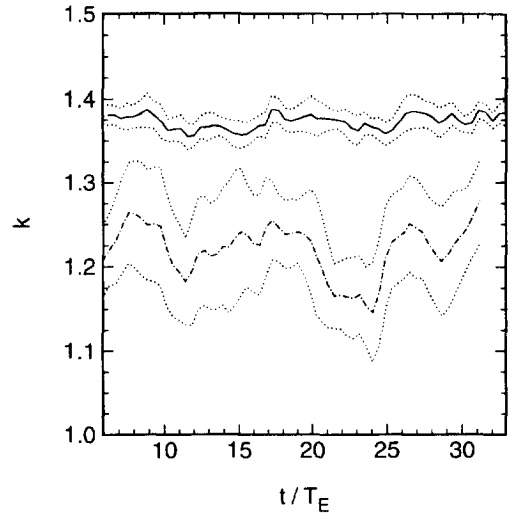

Fig. 13. Evolution of kinetic energy, showing decreased variability for the new forcing scheme. ———, run 32D.3; – · –, run 32.3; · · ·, 90% confidence intervals. Data for run 32.3 is from Overholt and Pope [15].

Finally, one of the quantities most affected by this forcing is the kinetic energy since it is so closely related to the energy spectrum. Figure 13 compares the evolution of k for runs 32.3 and 32D.3 with their confidence intervals and the difference is quite marked.

Two elements that are essential to natural forcing (as we have defined it) are: (1) the shape of the entire spectrum; and (2) the details of how energy is actually added. This second point was addressed in the formulation of the forcing method, specifically Equation (5). Runs 64DL and 64DLL give us a first look at how the shape of the simulated spectrum or fraction of energy captured affects the simulation statistics. Since increasing E_L^* decreases the size of the integral scales, the two-point spatial correlation will be different for each of these runs. Figures 14 and 15 show two of these correlations. It is encouraging to see that the transverse correlation (Fig. 14) fully returns to zero at the edges of the domain for the run having the smallest integral-scale sizes and the longitudinal correlation nearly does so as well.

A number of other scaled quantities were examined for these runs with no obvious differences seen between the results. Apparently, the results are not sensitive to changes in E_L^* on the order of 5% as considered here.

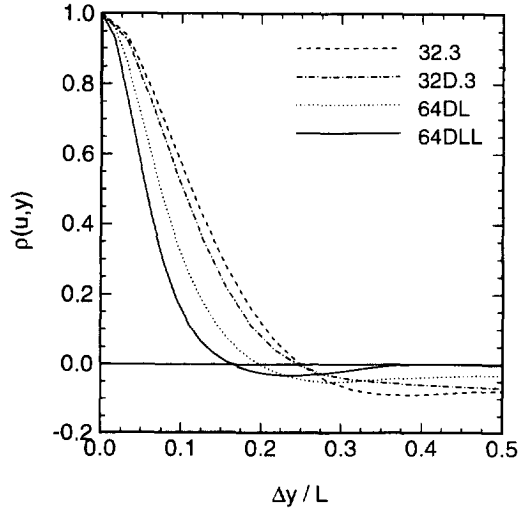

Fig. 14. Two-point spatial correlation of u-velocity in the y-direction. Data for run 32.3 is from Overholt and Pope [15].

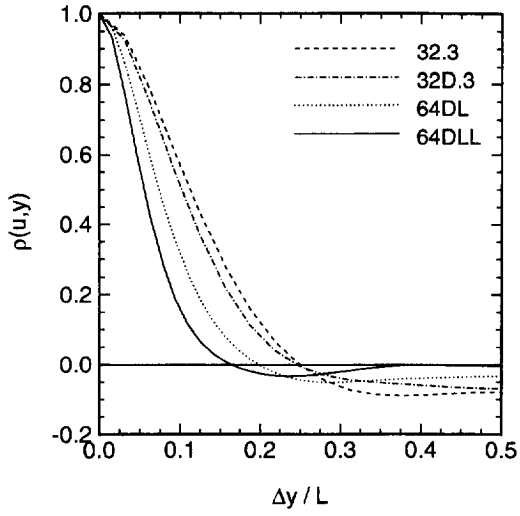

Fig. 15. Two-point spatial correlation of v-velocity in the y-direction. Data for run 32.3 is from Overholt and Pope [15].

4. CONCLUSIONS

A dynamic, deterministic forcing scheme for DNS has been developed which has a number of significant advantages over stochastic forcing and previous deterministic schemes and no apparent disadvantages. It produces an excellent representation of the energy-containing range of the energy spectrum and smaller statistical variability for most quantities. It also is physically more natural and has intuitive forcing parameters.

The forcing parameters are shown to be grid-independent and to ably control the dynamics of the forced system, which behaves like a mass–spring damper. The velocity and scalar fields quickly reach stationarity from any reasonable initial condition. A given spectrum is required to force to, and the general model spectrum of Pope [19] is a good choice. Not only does it accurately represent grid turbulence, it is also easy to calculate and use in this context.

Comparisons with the stochastic results of Overholt and Pope [15] yield virtually identical results, with many quantities having smaller confidence intervals. The similarity of the two results shows that the use of large-scale forcing in DNS at these Reynolds numbers is justified and the decreased variability shows that this new forcing method holds promise as a valuable tool in obtaining more precise DNS data in the future.

Acknowledgements—We gratefully acknowledge support from the Department of Energy, grant number DE-FG02-90ER 14128. Supercomputing resources were provided by the Cornell Theory Center, which receives major funding from NSF and New York State. Thanks also to our Theory Center consultant, Dr John Zollweg, for his assistance.

REFERENCES

1. Kolmogorov, A. N., Local structure of turbulence in an incompressible field at very high Reynolds numbers. *C.R. Acad. Sci. USSR*, 1941, **30**, 301–305.
2. Siggia, E. D. and Patterson, G. S., Intermittency effects in a numerical simulation of stationary three-dimensional turbulence. *Journal of Fluid Mechanics*, 1978, **86**, 567–592.
3. She, Z.-S., Jackson, E. and Orszag, S. A., Statistical aspect of vortex dynamics in turbulence In *New Perspectives in Turbulence*, ed. L. Sirovich. Springer, Berlin, 1991.
4. Chen, S., Doolen, G. D., Kraichnan, R. H. and She, Z.-S., On statistical correlations between velocity increments and locally averaged dissipation in homogeneous turbulence. *Physics of Fluids A*, 1993, **5**(2), 458–463.
5. Kerr, R. M., Theoretical Investigation of a Passive Scalar such as Temperature in Isotropic Turbulence. PhD thesis, Cornell University, 1981.
6. Vincent, A. and Meneguzzi, M., The spatial structure and statistical properties of homogeneous turbulence. *Journal of Fluid Mechanics*, 1991, **225**, 1–20.
7. Siggia, E. D., Numerical study of small-scale intermittency in three-dimensional turbulence. *Journal of Fluid Mechanics*, 1981, **107**, 375–406.
8. Holzer, M. and Siggia, E. D., Turbulent mixing of a passive scalar. *Physics of Fluids*, 1994, **6**(5), 1820–1837.
9. Pumir, A., A numerical study of the mixing of a passive scalar in three-dimensions in the presence of a mean gradient. *Physics of Fluids*, 1994, **6**(6), 2118–2132.

10. Eswaran, V. and Pope, S. B., An examination of forcing in direct numerical simulations of turbulence. *Computers and Fluids*, 1988, **16**(3), 257–278.
11. Yeung, P. K. and Pope, S. B., Lagrangian statistics from direct numerical simulations of isotropic turbulence. *Journal of Fluid Mechanics*, 1989, **207**, 531–586.
12. Ruetsch, G. R. and Maxey, M. R., Small-scale features of vorticity and passive scalar fields in homogeneous isotropic turbulence. *Physics of Fluids A*, 1991, **3**(6), 1587–1597.
13. Ruetsch, G. R. and Maxey, M. R., The evolution of small-scale structures in homogeneous isotropic turbulence. *Physics of Fluids A*, 1992, **4**(12), 2747–2760.
14. Lee, Y. Y. and Pope, S. B., Nonpremixed turbulent reacting flow near extinction. *Combustion and Flame*, 1995, **101**, 501–528.
15. Overholt, M. R. and Pope, S. B., DNS of a passive scalar with imposed mean gradient in isotropic turbulence. *Physics of Fluids*, 1996, **8**(11), 3128–3148.
16. Yakhot, V., Orszag, S. A. and Panda, R., Computational test of the renormalization group theory of turbulence. *Journal of Scientific Computing*, 1988, **3**(2), 139–147.
17. Rogallo, R. S., Numerical experiments in homogeneous turbulence. Technical Report 81315, NASA Technical Memorandum, 1981.
18. Eswaran, V. and Pope, S. B., Direct numerical simulations of the turbulent mixing of a passive scalar. *Physics of Fluids*, 1988, **31**(3), 506–520.
19. Pope, S. B., *Turbulent Flows*. Cambridge University Press, Cambridge, UK (to be published).
20. Saddoughi, S. G. and Veeravalli, S. V., Local isotropy in turbulent boundary layers at high Reynolds number. *Journal of Fluid Mechanics*, 1994, **268**, 333–372.
21. Comte-Bellot, G. and Corrsin, S., Simple Eulerian time correlation of full- and narrow-band velocity signals in grid-generated 'isotropic' turbulence. *Journal of Fluid Mechanics*, 1971, **48**, 273–337.

5. APPENDIX A

A linear stability analysis can be used to find the critical damping coefficient, α_c, as well as the stationary solution. To begin, a new variable, χ_κ, is defined as:

$$\chi_\kappa(t) \equiv \ln\left(\frac{E(\kappa;t)}{E_m(\kappa)}\right). \tag{A.1}$$

For the purposes of this analysis we only consider the lower-wave number range where κ is much less than κ_f and allow f_κ to take on both positive and negative values (i.e. to oscillate). Therefore, Z_f is approximately one and Equation (6) becomes:

$$\frac{df_\kappa(t)}{dt} = -\frac{\chi_\kappa(t)}{\tau} - \alpha\alpha_c f_\kappa(t). \tag{A.2}$$

From Equation (5) a relationship for $E(\kappa;t)$ can be derived as:

$$\frac{dE(\kappa;t)}{dt} = C(\kappa;t) + \frac{2f_\kappa(t)}{\tau}E(\kappa;t), \tag{A.3}$$

where

$$C(\kappa;t) \equiv \sum_{\text{shell }\kappa}[\hat{\mathbf{u}}^*\hat{\mathbf{a}} + \hat{\mathbf{u}}\hat{\mathbf{a}}^*], \tag{A.4}$$

is the contribution from the Navier–Stokes equations. For decaying isotropic turbulence we approximate:

$$\frac{1}{E(\kappa;t)}\frac{dE(\kappa;t)}{dt} = -\frac{bu'}{l}, \tag{A.5}$$

as independent of κ, where u' is the rms velocity and b is an unknown constant. The variables u' and l can be taken as constant and independent of κ if the range of wave numbers considered is sufficiently narrow and if the forcing maintains the stationarity of the velocity field. (Note: if Equation (A.5) is true over the entire energy-containing range, then $bu'k/l = \epsilon$.)

Rewriting Equation (A.3) in terms of χ_κ using Equation (A.5) yields:

$$\frac{d\chi_\kappa(t)}{dt} = -\frac{bu'}{l} + \frac{2f_\kappa(t)}{\tau}. \tag{A.6}$$

Equations (A.2) and (A.6) together constitute a two-dimensional linear system of equations that can be easily analyzed. The characteristic equation for this system is:

$$\lambda^2 + \alpha\alpha_c\lambda + \frac{2}{\tau^2} = 0, \tag{A.7}$$

with eigenvalue solutions

$$\lambda_{1,2} = \frac{-\alpha\alpha_c \pm \sqrt{\alpha^2\alpha_c^2 - 8/\tau^2}}{2}. \tag{A.8}$$

Critical damping, then, requires that:

$$\alpha_c \equiv \frac{2\sqrt{2}}{\tau}. \tag{A.9}$$

The fixed point or stationary values of f_κ and χ_κ can also be found. Setting Equation (A.6) equal to zero gives:

$$f_\kappa|_{\text{stat}} = \frac{b\tau u'}{2l}. \tag{A.10}$$

Setting Equation (A.2) equal to zero and substituting for $f_\kappa|_{\text{stat}}$ and α_c from Equations (A.10) and (A.9) gives:

$$\left(\frac{E}{E_m}\right)_{\text{stat}} = \exp^{-(\sqrt{2}\alpha b\tau u'/l)}. \tag{A.11}$$

Clearly the stationary solution for $E(\kappa;t)$ is dependent on both the damping and on the time scales.